Analysis and Reduction of Radiated EMI in High-Frequency GaN IC-based Active Clamp Flyback Converters

Juntao Yao, Yiming Li and Shuo Wang
Department of Electrical and Computer Engineering
University of Florida, Gainesville, FL, USA

Xiucheng Huang and Xiaofeng Lyu
Navitas Semiconductor, Inc.
El Segundo, CA, USA

***Abstract*- This paper investigates radiated electromagnetic interference (EMI) causes and solutions in high-frequency active-clamp flyback (ACF) using GaN ICs. GaN devices enable high-frequency operation which shrinks the passive component size and can potentially be more efficient. However, the increased spectrum of radiated EMI is a concern with a lack of readily-available solutions. This paper analyzes noise mechanisms by studying waveform and spectrum compositions, identifying major noise contributors. Near field couplings of the cable-converter electric couplings are identified as inducing the CM noise and bypassing the CM choke. This paper develops models to characterize the near field coupling effects on the radiated EMI. Noise reduction techniques including a shielding and grounding technique, a CLC pi-type CM filter are proposed and verified. Experimental verifications are performed on a GaN IC-based ACF power adapter and radiated EMI is brought into compliance.**

Index Terms—Electromagnetic interference (EMI), radiated EMI, radiated emission, active clamp flyback (ACF), near field

I. INTRODUCTION

In modern power electronics, fast-switching devices are pursued to reduce the size and improve the efficiency. Compared with traditional silicon devices, GaN increases the switching frequency beyond MHz, which can significantly reduce the size of passive components and increase power density [1-8]. The ACF converter is a ZVS soft-switching topology, which recycles the leakage and capacitive energy [9, 10]. Combined with GaN, the ACF converter switches efficiently near 1 MHz and is a game-changer for high power density and high-efficiency power adapters [11].

However, high switching frequency and compact layout create substantial challenges in EMI [9, 12-14]. High switching frequency pushes up the noise spectrum, which is a concern for radiated EMI. A small form-factor high-density layout and package results in parasitic noise couplings, which degrades EMI filter performance. An in-depth study is essential to overcome EMI challenges for high-frequency converters.

Some critical mechanisms of the radiated EMI have been revealed by the existing researches [14-16]. The long power cables attached to the power converter can be the dominant radiation antenna [14-16]. The antenna is driven by the noise generated by the power converter. In isolated power converters, the antenna can be driven by the voltage potential difference between the primary ground and the secondary ground, called CM terminal voltage. The CM terminal voltage results from the transformation of the switching noise through the transformer parasitics [14, 15, 17].

This research was supported by Navitas Semiconductor, Inc.

For reducing the radiated EMI, since the transformer is critical for the CM noise transformation, the improved transformer design can effectively reduce the CM noise and the radiated EMI in flyback converters [14]. High frequency lossy magnetic material based CM choke is another technique for reducing the radiated EMI [16]. The improved transformer design and the CM choke can reduce the conducted CM noise through the power converters and the resulted radiated EMI [14, 16]. In the application of the CM choke, due to the equivalent parallel capacitance (EPC), the effective frequency range of the CM choke is constrained [18-22]. Extensive researches focus on reducing the EPC by cancellation techniques [19-21, 23].

When the noise propagates through electromagnetic waves rather than through the conducted path, the near field coupling can impose substantial influence on EMI [24-26]. And since the development of high power density power converters makes the layout increasingly compact, near field coupling is an increasingly important topic in EMI researches [26-28].

This paper will analyze noise mechanisms and develop noise-reduction techniques. In the second section, the paper will analyze the waveform and spectrum compositions and identify major contributors to the high-frequency noise spectrum. In the third section, the near field coupling effect on the radiated EMI in ACF power converters will be investigated. In the fourth section, noise reduction techniques including the shielding and grounding techniques, and a CLC pi-type CM filter will be proposed and verified. Analytical investigations and experimental results are based on a 60 W GaN IC-based ACF PD power adapter.

II. NOISE SOURCE ANALYSES OF THE ACF WITH GAN POWER IC DEVICES

The schematic of a GaN IC-based ACF power adapter is shown in Fig. 1.

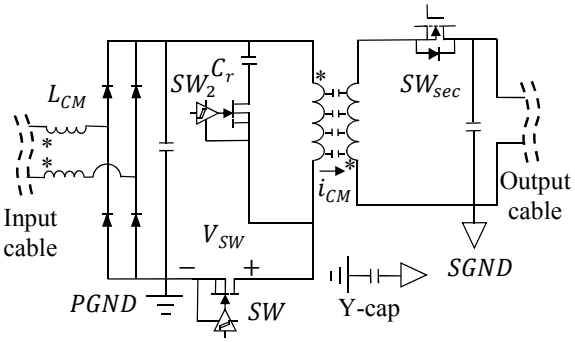

Fig. 1. GaN IC-based ACF power adapter with power cables attached

To analyze the noise sources, it is important to analyze the switching waveform and to identify critical parameters to the high-frequency noise spectrum.

Fig. 2 shows the measured waveform of the soft-switched ACF power adapter, with AC input 120 V 60 Hz, DC output 20 V / 3 A and switching frequency 450 kHz. Parasitic ringing is minimized compared with traditional flyback converter [10]. To identify the contributors to the high-frequency spectrum, the whole waveform is split to several components, as shown in Fig. 2 (a), including 1) the trapezoidal component consisting of rising and falling edges, 2) the clamping component, and other components like the conducting stage with zero dv/dt which almost has zero contribution to the high-frequency spectrum. Fig. 2 (b) shows that spectrum contributions from each component, which indicates that the clamping component including the minimized parasitic ringing is not a significant contributor to the high-frequency spectrum and that the trapezoidal component is the predominant contributor. Note that, due to the resolution of the captured time-domain data, the spectrum is shown up to 100 MHz [15].

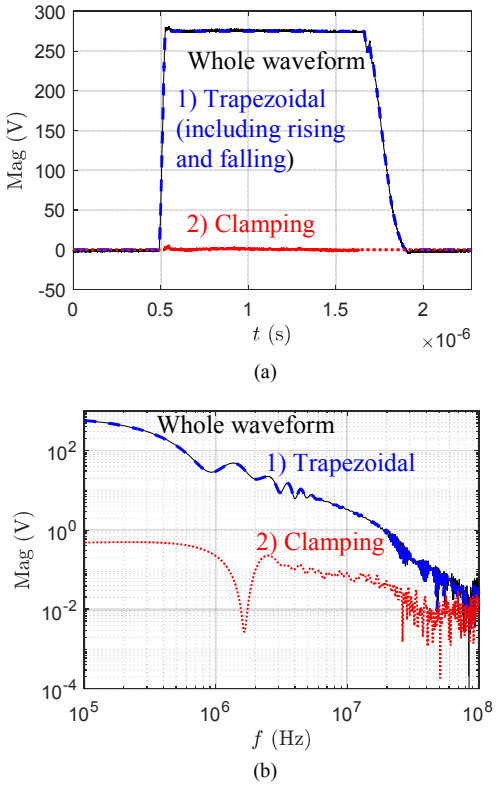

Fig. 2. Composition of switching-voltage waveforms and spectrums (a) composition of switching-voltage waveform (b) spectrums

The differential-mode pulsating voltages can transform into the CM noise through transformer parasitics, as shown in Fig. 3. In Fig. 3, V_{SW} represents the switching voltage, Z_{Trans1} and Z_{Trans2} represent the lumped impedances of the transformer parasitics [15]. Power converter's transformed CM noise acts as the excitation to drive the attached input and output power cables radiating to space [14]. Based on existing techniques, the switching behaviors, the transformer, and the CM choke are optimized [9] to reduce the CM noise and the resulted radiated EMI.

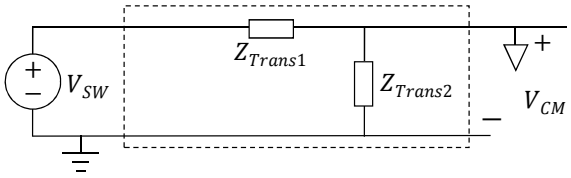

Fig. 3. CM model of the noise transformation from the switching pulsating voltage to the CM noise through the lumped impedances of the transformer parasitics

The relation between the CM noise and the radiation can be explained using the equivalent circuit as shown in Fig. 4, where R_r is the equivalent radiation resistance, R_L is the loss resistance of the power cables, X_A is the reactive component representing the near field energy [29], and $Z_{Antenna} = R_r + R_L + jX_A$ is the antenna's impedance. The power delivered to the antenna for radiation is

$$P_r = |I_{CM}|^2 R_r = \left(V_{CM} \cdot \frac{Z_{Antenna}}{Z_{CMConv}+Z_{Antenna}}\right)^2 \cdot R_r \quad (1)$$

where Z_{CMConv} is the equivalent CM impedance of the power converter. To estimate the radiated EMI intensity, the electric field intensity E is a measure. And the relation between the radiation power and the electric field intensity E, in the equivalent isotropic and uniform radiation case, is

$$P_r = \frac{E^2}{2\eta} \cdot 4\pi r^2 \quad (2)$$

i.e.

$$E = \sqrt{P_r \eta / 2\pi r^2} \quad (3)$$

where r is the distance between the radiation antenna and the observation point, η is the characteristic impedance $120\pi\ \Omega$. Note that in the uneven radiation case, given the directivity gain D, $E_{max} = \sqrt{D} \cdot E$.

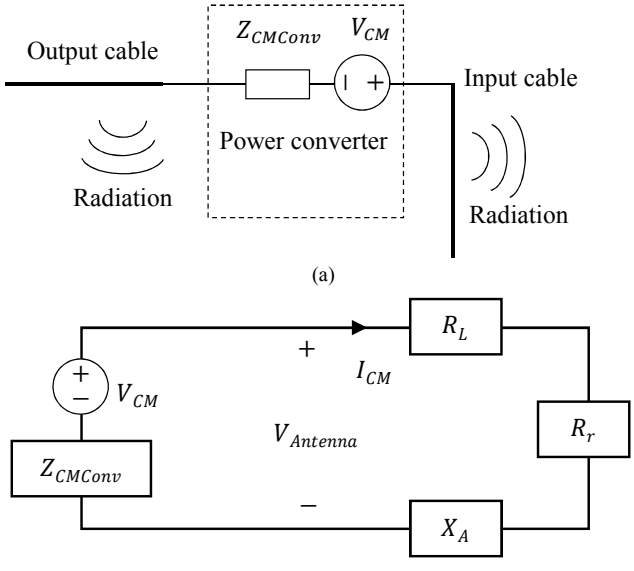

Fig. 4. Radiation from the power converter with power cables attached (a) radiation from the power cable antenna driven by the power converter's CM noise source (b) equivalent circuit of the radiation system

Based on (1)~(3), the electric field intensity

$$E = \left|\frac{Z_{Antenna}}{Z_{CMConv}+Z_{Antenna}}\right| \cdot \sqrt{\frac{(V_{CM})^2 \cdot R_r \cdot \eta}{2\pi r^2}} \quad (4)$$

where an index can be extracted to indicate the influence from the impedances on the radiated EMI

$$G_Z = \frac{Z_{Antenna}}{Z_{CMConv}+Z_{Antenna}} \quad (5)$$

Regarding the gain G_Z, Table I is listed to explain the difference before the application of the CM choke with high impedance at high frequencies. Based on Table I, G_Z can also represent the noise attenuation gain after the application of the CM choke.

Table. I. Antenna excitation gain before and after the application of CM choke

	Initial case, W/o CM choke	W/ CM choke
Z_{CMConv} in (30, 200) MHz	*Small* ($\ll 100\ \Omega$, $\ll Z_{Antenna}$)	Z_{LCM}, big ($\approx 1000\ \Omega$)
Gain G_Z	0 dB	$\frac{Z_{Antenna}}{Z_{LCM}+Z_{Antenna}}$

The impedances of the antenna and the CM choke are shown in Fig. 5. In the concerned frequency range (30, 200) MHz, the CM choke is resistive to dissipate the noise energy and to avoid the resonance with the antenna impedance.

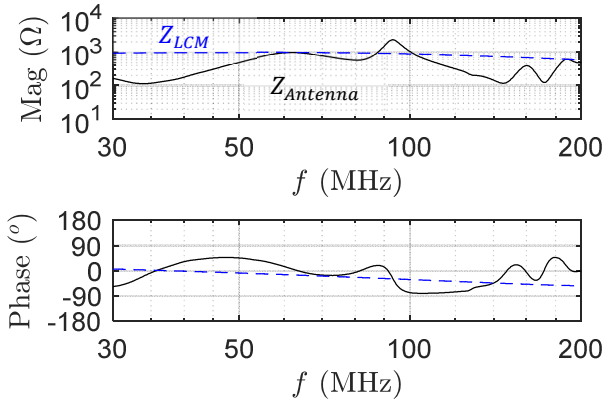

Fig. 5. Impedances of antenna and CM choke

Fig. 6 shows the curve of the expected noise attenuation gain after the application of the CM choke. According to Fig. 6, the application of the CM choke should be effective to reduce the noise in the concerned frequency range (30, 200) MHz. And the expected noise attenuation is over 6 dB in (30, 80) MHz.

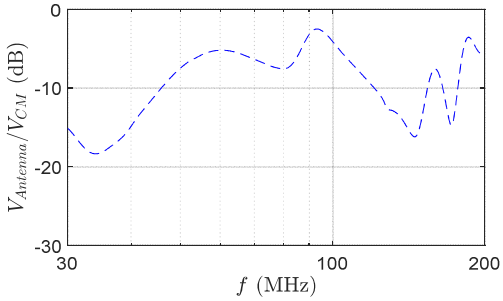

Fig. 6. Ideal noise attenuation gain by the CM choke

Radiated EMI is measured in a semi-anechoic chamber as shown in Fig. 7. The ACF power adapter, as the equipment under test (EUT), is arranged 3 meters away from the receiving antenna. The radiated EMI measurement results are shown in Fig. 8, which are over the limit of the standard EN55032. The CM choke has a limited noise reduction effect in (60, 80) MHz, which cannot reach the expected attenuation gain as shown in Fig. 6. It is essential to analyze the possible influential factors degrading the CM choke's noise reduction effect and to propose solutions for further reducing the radiated EMI to make it in compliance with the standard.

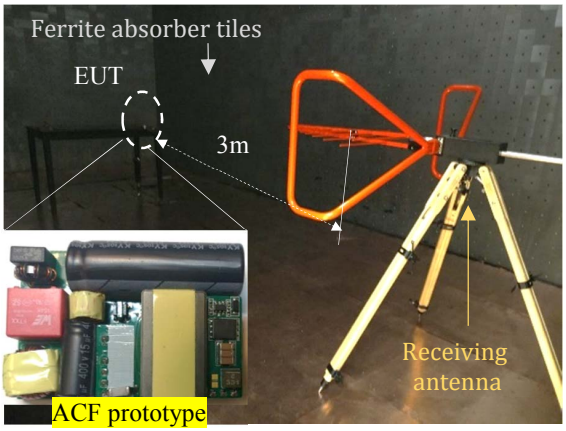

Fig. 7. Radiated EMI measurement for the ACF in a semi-anechoic chamber

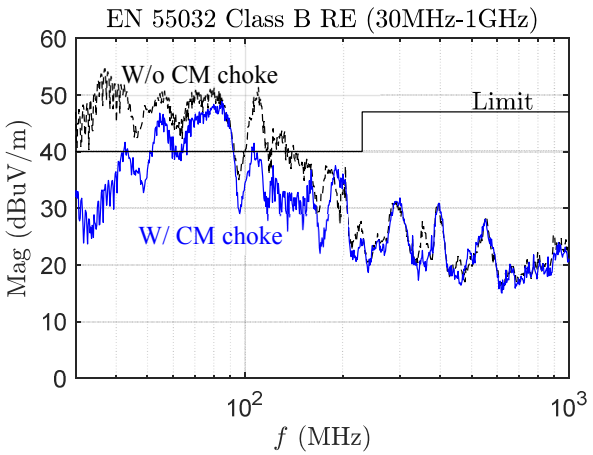

Fig. 8. Radiated EMI measurement results W/o and W/ the CM choke applied

III. Radiated EMI Models of an ACF with Near Field Coupling Effect Included

Fig. 9 shows an equivalent circuit of the radiated EMI model of the ACF without the consideration of near field couplings based on existing researches [14],where Z_{Trans1} and Z_{Trans2} are transformer's lumped CM impedances, Z_{Ycap} is the Y-cap's impedance, Z_{LCM} is the CM choke's impedance. However, in the high-power density ACF power adapters with the layout increasingly compact, near field couplings and their effects on EMI are important. Based on experimental investigations, the electric near field coupling is identified as influential to the study case of a GaN IC-based ACF.

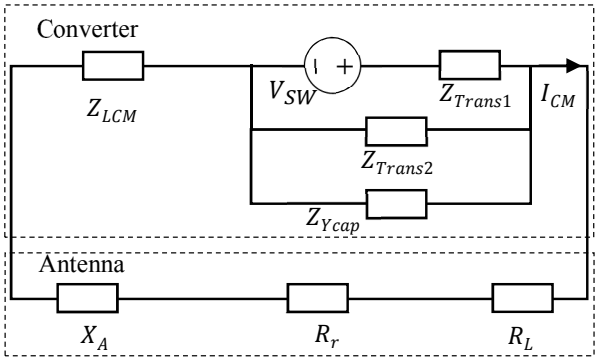

Fig. 9. Radiated EMI model of the ACF without the consideration of near field couplings

In order to include all the influential electric near couplings between CM circuit nodes within the ACF power converter, the CM circuit nodes are marked, as shown in Fig. 10. And the CM nodes are listed in Table II.

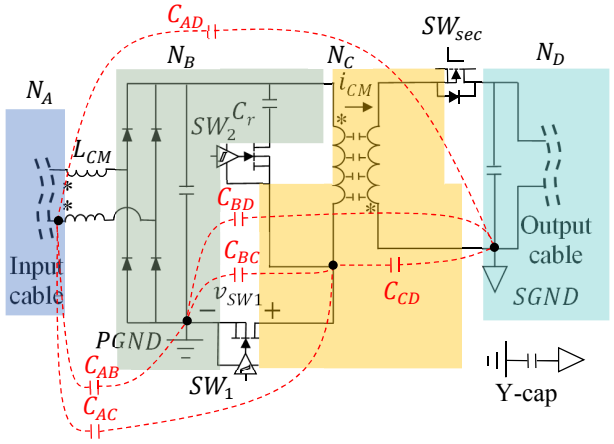

Fig. 10. CM nodes in the ACF

Table. II. List of CM nodes in the ACF

CM node number	Corresponding ACF circuit area
N_A	Input cable before CM choke
N_B	DC side after CM choke
N_C	Areas with pulsating voltages
N_D	DC output and output cable

And the influences of the different couplings on the CM noise and the radiated EMI are discussed as listed in Table III.

Table. III. List of parasitic couplings between CM nodes

No.	Between CM nodes	Analyses about the significance
1	N_A and N_C	The noise injected to the power cable can cause the radiated EMI.
2	N_A and N_B	Parasitic capacitance bypassing the CM choke.
3	N_A and N_D	It is the antenna formed by the power cables, not the coupling related to the power converter. If additional capacitor (or parasitic capacitance) is added between A and D, it can act as the equivalent Y-cap, which is helpful for noise reduction.
4	N_B and N_C	Since it is in parallel with the switching device SW_1, it does not contribute to the CM noise.
5	N_B and N_D	Since the small parasitic capacitance is connected in parallel with a big Y-cap, it has negligible influence.
6	N_C and N_D	Displacement current injection can cause noise currents, which is negative causing the radiated EMI. But the influence is not significant since the secondary side does not have the CM choke and no bypassing effect can be induced to the secondary side.

As listed in Table. III, the No. 1 and No. 2 electric near field couplings can significantly impact the radiated EMI, which will be analyzed respectively in this section.

A. Between N_A and N_C, couplings between the pulsating node and the input cable

The radiated EMI model of the ACF can be improved from Fig. 9 to Fig. 11, with the influential electric near field couplings included. Based on the model shown in Fig. 11, the transfer gain

$$G_{Z\_W\_CAC\_CAB} = \frac{V_{Antenna}}{V_{SW}} = \left(\frac{Z_{WB2}}{Z_{WB1}+Z_{WB2}} - \frac{Z_{WB4}}{Z_{WB3}+Z_{WB4}}\right) \quad (6)$$

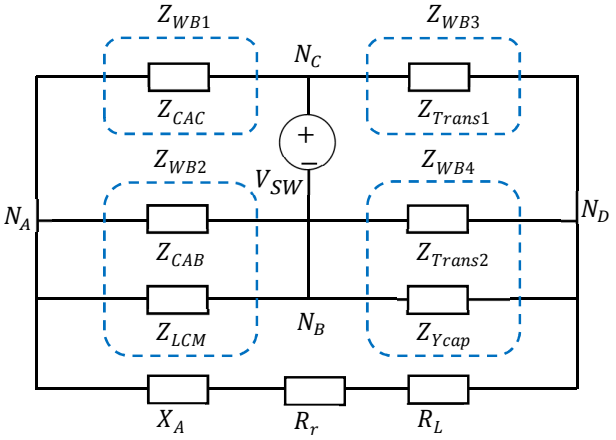

Fig. 11. Radiated EMI model of the power converter with coupling parasitics

To quantify the electric near field couplings, the coupling parasitics need to be extracted. To emulate the pulsating voltage distribution along the transformer windings and along the PCB traces, the two-port S-parameter method is applied, as shown in Fig. 12. Port 1 is the transmitting port which generates the incident microwave and imposes pulsating voltages to the transformer winding and the PCB traces. Port 2 is the receiving port that receives the transformed power. Based on the testing results of the S-parameters, a π network can be extracted [15], as shown in Fig. 13, where Z_{π_3} is the lumped impedance to characterize the equivalent coupling parasitic impedance Z_{CAC} between the pulsating node and the victim node of the input power cable, as

$$Z_{CAC} = Z_{\pi\_3} \quad (7)$$

The lumped impedance Z_{CAC} representing the coupling parasitics is extracted as shown in Fig. 14, as 5.69 pF. At high

frequencies (especially >60 MHz), Z_{WB2} is predominantly capacitive (~6.60 pF) because of CM inductor's and the power converter's parasitic capacitances. Z_{WB4} is the impedance of 1.59 nF and Z_{WB3} is the impedance of 1.59 pF. In (6), the term $Z_{WB2}/(Z_{WB1}+Z_{WB2})$ is much larger than $Z_{WB4}/(Z_{WB3}+Z_{WB4})$and hereby predominates $G_{Z\_W\_CAC\_CAB}$. As a result, the couplings between N_A and N_C can undermine the noise reduction effectiveness of the balanced transformer and the CM choke.

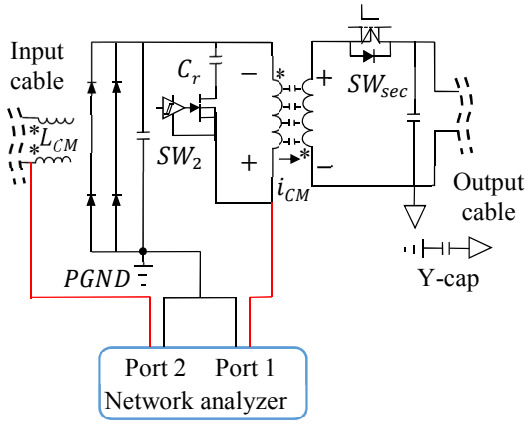

Fig. 12. Diagram of the coupling parasitic extraction method

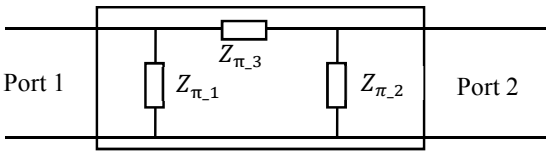

Fig. 13. π model of the extracted circuit network

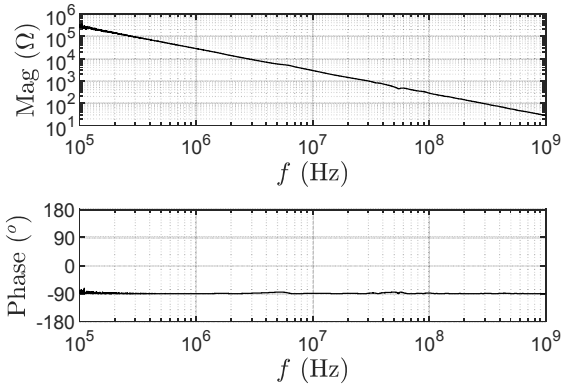

Fig. 14. Extracted coupling parasitics impedance Z_{CAC}

In order to verify the impacts of the couplings between N_A and N_C, an experiment is conducted as shown in Fig. 15. The pulsating node N_C is shielded and grounded to $SGND$. The radiated EMI is measured and compared with the original ACF power converter, as shown in Fig. 15 (b). The radiated EMI is reduced, especially >60 MHz. It should be pointed out that, the shielding should be grounded to SGND rather than PGND. Otherwise, when the shielding is connected to PGND, the electric near field couplings between the input cable and the shielding can cause an EPC which can be added to C_{AB} and bypass the CM choke. As a result, when the shielding is connected to PGND, the radiated EMI is not reduced. The bypassing effect of C_{AB} will be analyzed in the next sub-section.

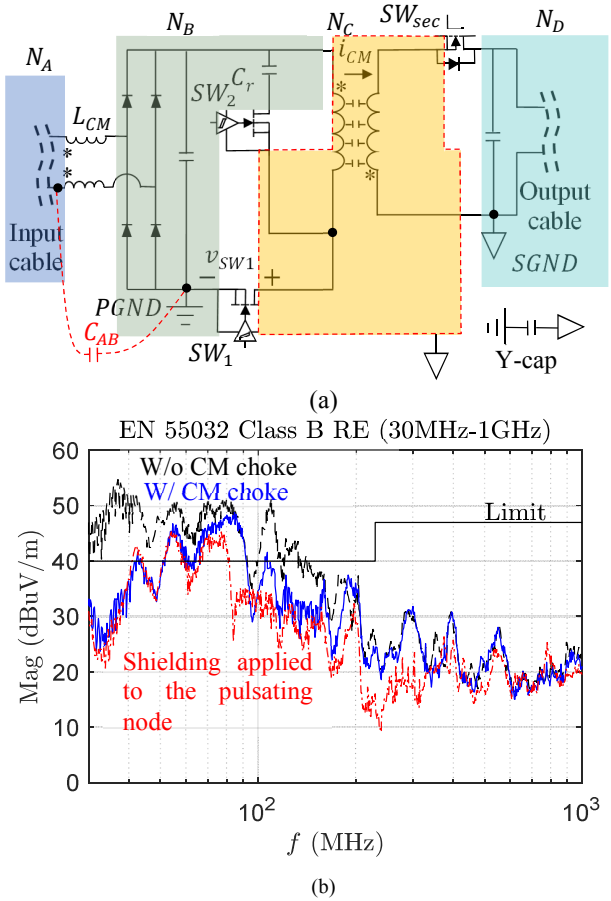

Fig. 15. Investigation of shielding applied to the pulsating node (a) shielding applied to the pulsating node (b) radiated EMI results

B. Between N_A and N_C, bypassing impact to EMI filter

After the shielding applied to the pulsating node N_C, the effect of the coupling between N_A and N_C is eliminated. Another near field coupling mechanism emerges as an influential factor for degrading the CM choke's noise reduction effect. The electric near couplings between node N_A and N_B can cause EPC. And the EPC can cause small impedances at high frequencies and can bypass the CM choke, as shown in Fig. 16.

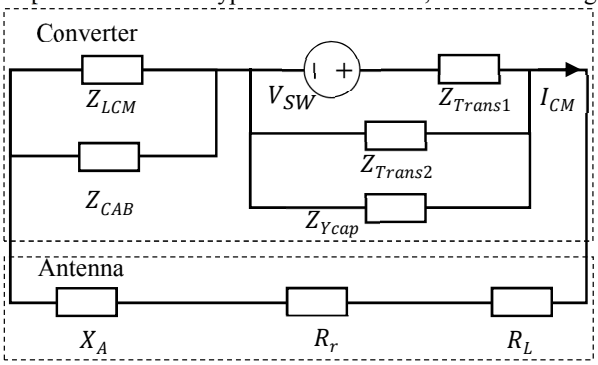

Fig. 16. Bypassing parasitic impedance considered in the equivalent circuit of CM noise and radiation in the ACF

Based on the extracted impedances as shown in Fig. 17, the cable-converter coupling can cause the EPC bypassing the CM choke and degrading the noise reduction effect.

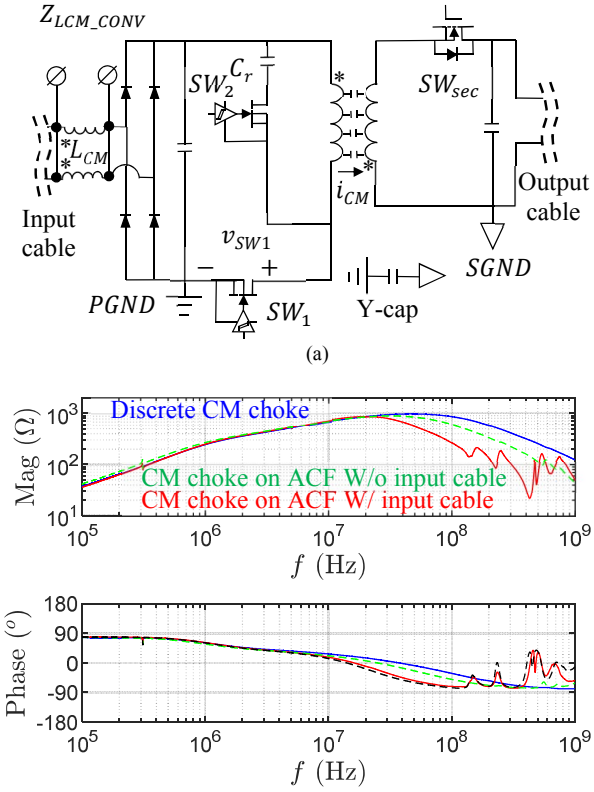

Fig. 17. CM choke impedances, discrete case and on the ACF board case (a) impedance extraction at CM choke terminals (b) extracted impedances

When $Z_{CAB} \ll Z_{LCM}$, the CM choke is bypassed by the cable-converter coupling parasitics. And the noise attenuation gain is not $G_Z = \frac{Z_{Antenna}}{Z_{LCM}+Z_{Antenna}}$ but

$$G_{Z\_W\_CAB} = \frac{Z_{Antenna}}{Z_{LCM}||Z_{CAB}+Z_{Antenna}} \quad (8)$$

and the noise reduction effect of the CM choke is degraded. Techniques to eliminate the effect of electric near field couplings will be investigated in section IV.

IV. Noise Reduction Techniques

CM choke's noise reduction effect is degraded by the near field couplings based on the analyses in section III. Analyses and solution techniques for eliminating the near field coupling effect are important. Moreover, after eliminating the near field coupling effect, to reduce the radiated EMI in compliance with the standard, further noise reduction techniques need to be explored.

A. Coupling effect elimination: a shielding-sec-grounding technique

To eliminate the two sorts of coupling effects 1) coupling between the pulsating node and the input cable, 2) bypassing effect to EMI filter, the undesired coupling path needs to be blocked or changed, the converter is shielded, and the shielding is connected to SGND, called as the shielding-sec-grounding technique, as shown in Fig. 18. It should be pointed out that, the whole converter shielding should be grounded to SGND rather than PGND. Otherwise, when the shielding is connected to PGND, the electric near field coupling between the input cable and the shielding can cause an EPC C'_{AB} which can be larger than C_{AB}. As a result, when the shielding is connected to PGND, the radiated EMI can be even worse than the original power converter without shielding applied.

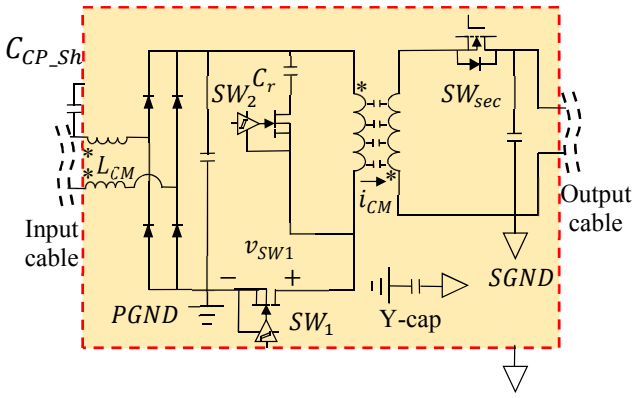

Fig. 18. ACF with shielding and the shielding connected to the secondary ground

This shielding-sec-grounding technique has three major benefits including 1) blocking the electric near field couplings between the pulsating nodes and the power cable, 2) blocking the electric near field couplings causing the bypassing effect, after the electric near field having been changed to SGND for avoiding the bypassing EPC, 3) equivalent Y-cap between the input power cable and the shielding grounded to SGND.

About the third benefit, as shown in Fig. 19, the coupling path is changed to SGND, and the noise reduction gain is

$$G_{Z\_Sh} = \frac{Z_{Antenna}||Z_{CP\_Sh}}{Z_{LCM}+Z_{Antenna}||Z_{CP\_Sh}} \quad (9)$$

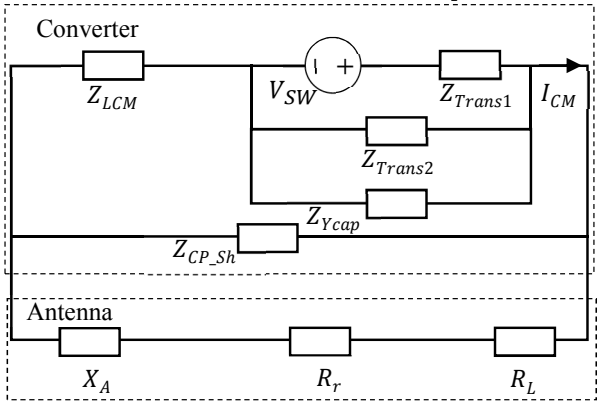

Fig. 19. Circuit model of CM noise with converter shielding and the corresponding cable-shielding coupling parasitic impedance

In other words, a low impedance branch connected in parallel with the antenna is helpful to reduce the voltage drop as the excitation for the antenna radiation. Accordingly, the radiated EMI is reduced, as shown in Fig. 20. The third benefit of the shielding-sec-grounding technique stimulates the idea of adding a capacitor in parallel with the antenna for improving the CM filter topology and for further reducing the radiated EMI, which will be explained in the next sub-section.

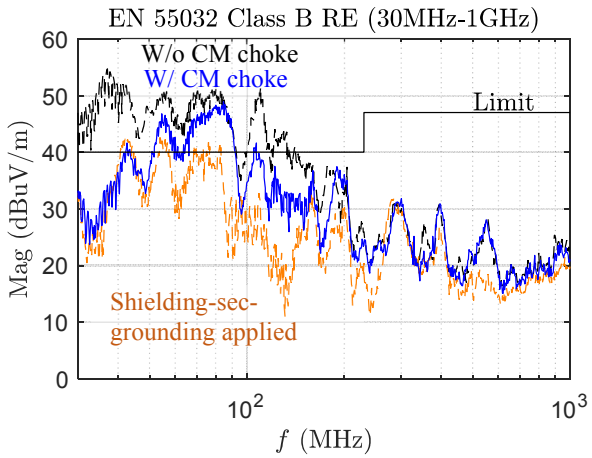

Fig. 20. Investigation of shielding's effect on radiated EMI

B. A CLC pi-type CM filter for reducing radiated EMI in power converters

A CLC pi-type CM filter is proposed in combination with the shielding-sec-grounding technique for reducing the radiated EMI, as shown in Fig. 21. And the noise reduction gain is

$$G_{Z\_PiCM} = \frac{Z_{Antenna}||Z_{Ycap2}}{Z_{LCM}+Z_{Antenna}||Z_{Ycap2}} \quad (10)$$

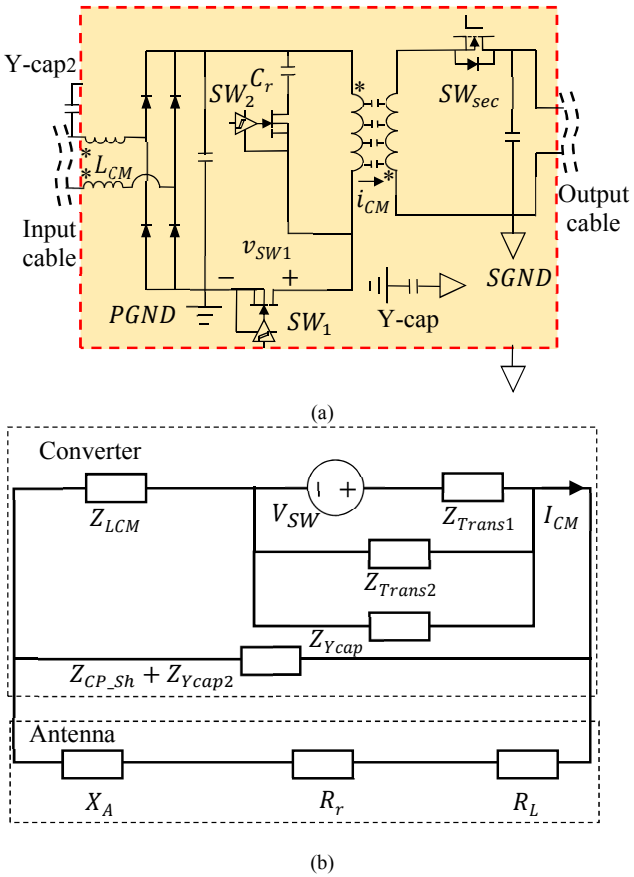

Fig. 21. The proposed CLC pi-type CM filter combined with the shielding-sec-grounding technique (a) application in the ACF (b) equivalent circuit

Based on the impedance mismatch theorem in the EMI filter design, the inserted Y-cap2 needs to produce a smaller impedance than the antenna impedance. For example, a surface-mount device (SMD) 110 pF capacitor is selected given the impedance comparison shown in Fig. 22.

With the application of the proposed CLC CM EMI filter, the noise reduction gain is improved as compared with the case with merely the CM choke, as demonstrated by small-signal transfer gain extractions shown in Fig. 23. And the radiated EMI is effectively reduced, as shown in Fig. 24, which further verifies the effectiveness of the proposed CLC CM filter for reducing the radiated EMI in ACF power converters.

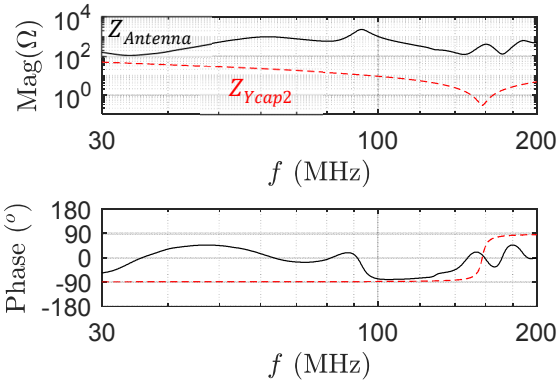

Fig. 22. Impedances of the antenna and the Y-cap2 included in the proposed CLC CM filter

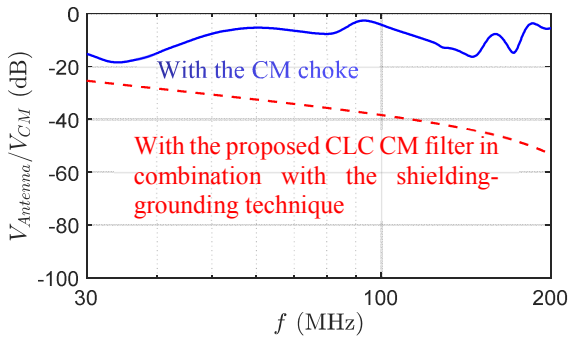

Fig. 23. Extracted transfer gains representing noise reduction effects

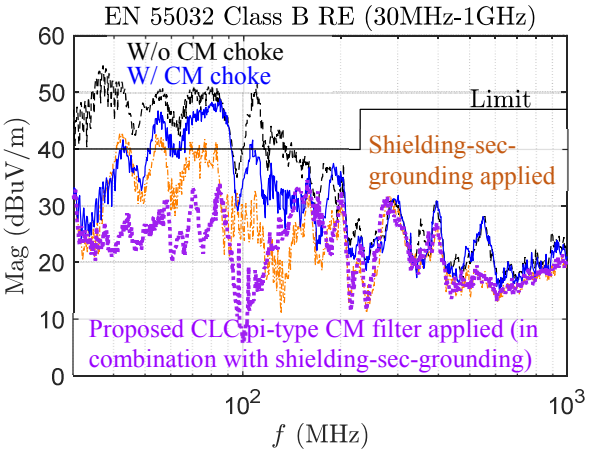

Fig. 24. Radiated EMI results before and after the application of the noise reduction techniques

With the shielding-sec-grounding technique and the CLC pi-type CM filter applied, the radiated EMI in the ACF is brought into compliance with the standard EN 55032.

V. CONCLUSIONS

This paper analyzes and reduces radiated EMI in high-frequency GaN IC-based ACF power adapters. The near field coupling effect on the radiated EMI is analyzed. Noise reduction techniques are proposed and verified.

GaN IC-based ACF minimizes the transient ringing and its contribution to the high-frequency noise spectrum. The trapezoidal component of the ACF switching voltage is the dominant contributor to the high-frequency noise spectrum.

Cable-converter electric near field coupling is identified as a negative factor degrading the noise reduction effect of the CM choke. Cable-converter electric near field coupling models are developed and verified.

Moreover, several noise reduction techniques are proposed and verified to bring the GaN IC-based ACF in compliance with the radiated EMI standard. (a) The proposed shielding-sec-grounding technique can eliminate the effect of cable-converter couplings and reduce the radiated EMI. (b) The proposed CLC pi-type CM filter in combination with the shielding-sec-grounding technique can improve the noise attenuation gain and reduce the radiated EMI.

REFERENCES

[1] X. Huang, Z. Liu, F. C. Lee, and Q. Li, "Characterization and Enhancement of High-Voltage Cascode GaN Devices," *IEEE Transactions on Electron Devices,* vol. 62, pp. 270-277, 2015.

[2] X. Huang, Z. Liu, Q. Li, and F. C. Lee, "Evaluation and Application of 600 V GaN HEMT in Cascode Structure," *IEEE Transactions on Power Electronics,* vol. 29, pp. 2453-2461, 2014.

[3] D. Cao, X. Lyu, Y. Li, Z. Ni, J. Johnson, S. Jiang, *et al.*, "An ultra efficient composite modular power delivery architecture for solar farm and data center," in *2018 IEEE Applied Power Electronics Conference and Exposition (APEC)*, 2018, pp. 73-80.

[4] X. Lyu, Y. Li, D. Cao, S. Jiang, and C. Nan, "Comparison of GaN based switched-tank converter and cascaded voltage divider," in *2017 IEEE 5th Workshop on Wide Bandgap Power Devices and Applications (WiPDA)*, 2017, pp. 158-164.

[5] B. Li, Q. Li, F. C. Lee, Z. Liu, and Y. Yang, "A High-Efficiency High-Density Wide-Bandgap Device-Based Bidirectional On-Board Charger," *IEEE Journal of Emerging and Selected Topics in Power Electronics,* vol. 6, pp. 1627-1636, 2018.

[6] B. Zhang and S. Wang, "An Overview of Wide Bandgap Power Semiconductor Device Packaging Techniques for EMI Reduction," in *2018 IEEE Symposium on Electromagnetic Compatibility, Signal Integrity and Power Integrity (EMC, SI & PI)*, 2018, pp. 297-301.

[7] S. Zhao, X. Zhao, A. Dearien, Y. Wu, Y. Zhao, and H. A. Mantooth, "An Intelligent Versatile Model-Based Trajectory Optimized Active Gate Driver for Silicon Carbide Devices," *IEEE Journal of Emerging and Selected Topics in Power Electronics,* pp. 1-1, 2019.

[8] S. Zhao, A. Dearien, Y. Wu, C. Farnell, A. U. Rashid, F. Luo, *et al.*, "Adaptive Multi-Level Active Gate Drivers for SiC Power Devices," *IEEE Transactions on Power Electronics,* pp. 1-1, 2019.

[9] X. Huang, J. Feng, W. Du, F. C. Lee, and Q. Li, "Design consideration of MHz active clamp flyback converter with GaN devices for low power adapter application," in *2016 IEEE Applied Power Electronics Conference and Exposition (APEC)*, 2016, pp. 2334-2341.

[10] L. Xue and J. Zhang, "Highly Efficient Secondary-Resonant Active Clamp Flyback Converter," *IEEE Transactions on Industrial Electronics,* vol. 65, pp. 1235-1243, 2018.

[11] F. C. Lee, "Keynote 1: Is GaN a Game Changing Device ?," in *2014 16th International Power Electronics and Motion Control Conference and Exposition*, 2014, pp. 8-14.

[12] Y. Zhang, S. Wang, and Y. Chu, "Investigation of Radiated Electromagnetic Interference for an Isolated High-Frequency DC–DC Power Converter With Power Cables," *IEEE Transactions on Power Electronics,* vol. 34, pp. 9632-9643, 2019.

[13] H. Chen, T. Wang, L. Feng, and G. Chen, "Determining Far-Field EMI From Near-Field Coupling of a Power Converter," *IEEE Transactions on Power Electronics,* vol. 29, pp. 5257-5264, 2014.

[14] J. Yao, Y. Li, H. Zhao, S. Wang, Q. Wang, Y. Lu, *et al.*, "Modeling and Reduction of Radiated Common Mode Current in Flyback Converters," in *2018 IEEE Energy Conversion Congress and Exposition (ECCE)*, 2018, pp. 6613-6620.

[15] J. Yao, S. Wang, H. Zhao, Y. Zhang, Q. Wang, Y. Lu, *et al.*, "Measurement Techniques of CM Currents, Impedance and Voltages for Radiated EMI in Isolated Power Converters," in *2018 IEEE Symposium on Electromagnetic Compatibility, Signal Integrity and Power Integrity (EMC, SI & PI)*, 2018, pp. 438-443.

[16] J. Yao, Y. Li, H. Zhao, and S. Wang, "Design of CM Inductor Based on Core Loss for Radiated EMI Reduction in Power Converters," in *2019 IEEE Applied Power Electronics Conference and Exposition (APEC)*, 2019, pp. 2673-2680.

[17] H. Zhao, J. Yao, and S. Wang, "A Universal DM/CM Physical Model for Power Transformer EMI Analysis within both Conducted and Radiated Frequency Ranges," in *2018 IEEE Energy Conversion Congress and Exposition (ECCE)*, 2018, pp. 6592-6599.

[18] C. Rengang, J. D. v. Wyk, W. Shuo, and W. G. Odendaal, "Improving the Characteristics of integrated EMI filters by embedded conductive Layers," *IEEE Transactions on Power Electronics,* vol. 20, pp. 611-619, 2005.

[19] S. Wang, F. C. Lee, W. G. Odendaal, and J. D. v. Wyk, "Improvement of EMI filter performance with parasitic coupling cancellation," *IEEE Transactions on Power Electronics,* vol. 20, pp. 1221-1228, 2005.

[20] S. Wang, F. C. Lee, and J. D. v. Wyk, "Inductor winding capacitance cancellation using mutual capacitance concept for noise reduction application," *IEEE Transactions on Electromagnetic Compatibility,* vol. 48, pp. 311-318, 2006.

[21] S. Wang, F. C. Lee, J. D. v. Wyk, and J. D. v. Wyk, "A Study of Integration of Parasitic Cancellation Techniques for EMI Filter Design With Discrete Components," *IEEE Transactions on Power Electronics,* vol. 23, pp. 3094-3102, 2008.

[22] Y. Liu, K. Y. See, J. Lai, K. J. Tseng, Y. Liu, C. F. Tong, *et al.*, "FEM modelling of three-phase common mode choke for performance evaluation," in *2016 Asia-Pacific International Symposium on Electromagnetic Compatibility (APEMC)*, 2016, pp. 96-99.

[23] S. Wang, C. Rengang, J. D. V. Wyk, F. C. Lee, and W. G. Odendaal, "Developing parasitic cancellation technologies to improve EMI filter performance for switching mode power supplies," *IEEE Transactions on Electromagnetic Compatibility,* vol. 47, pp. 921-929, 2005.

[24] Y. Chu, S. Wang, J. Xu, and D. Fu, "EMI reduction with near field coupling suppression techniques for planar transformers and CM chokes in switching-mode power converters," in *2013 IEEE Energy Conversion Congress and Exposition*, 2013, pp. 3679-3686.

[25] K. Takahashi, Y. Murata, Y. Tsubaki, T. Fujiwara, H. Maniwa, and N. Uehara, "Mechanism of Near-Field Coupling Between Noise Source and EMI Filter in Power Electronic Converter and Its Required Shielding," *IEEE Transactions on Electromagnetic Compatibility,* vol. 61, pp. 1663-1672, 2019.

[26] Y. Li, S. Wang, H. Sheng, and S. Lakshmikanthan, "Investigate and Reduce Capacitive Couplings in a Flyback Adapter with a DC-Bus Filter to Reduce EMI," *IEEE Transactions on Power Electronics,* pp. 1-1, 2019.

[27] F. Costa, C. Gautier, B. Revol, J. Genoulaz, and B. Démoulin, "Modeling of the near-field electromagnetic radiation of power cables in automotives or aeronautics," *IEEE Transactions on Power Electronics,* vol. 28, pp. 4580-4593, 2013.

[28] H. Chen and Z. Qian, "Modeling and Characterization of Parasitic Inductive Coupling Effects on Differential-Mode EMI Performance of a Boost Converter," *IEEE Transactions on Electromagnetic Compatibility,* vol. 53, pp. 1072-1080, 2011.

[29] C. Balanis, *Antenna Theory: Analysis and Design*: Wiley Blackwell, 2016.